

Effect of Residual Stress in Surface Layer on Deformation of Elastic-Plastic Layered Media Under Normal and Sliding Contact Traction

N. Ye, Graduate Student

K. Komvopoulos, Professor, Fellow ASME

Department of Mechanical Engineering
University of California
Berkeley, CA 94720

Abstract

Deformation of layered media under normal and sliding contact traction with residual stress in the top layer was analyzed with the finite element method. A three-dimensional finite element model of a rigid spherical asperity indenting and sliding over an elastic-plastic layered medium was developed and validated by contrasting finite element results with analytical solutions of the surface stresses for an elastic homogeneous half-space. A series of simulations were performed for varying magnitude of residual stress in the layer and two different coefficients of friction. Deformation in the layered medium is interpreted in light of the dependence of von Mises equivalent stress, first principal stress, and equivalent plastic strain on the magnitudes of residual stress in the top layer and coefficient of friction. The effect of residual stress on plastic flow and microcracking in the layered medium is discussed in the context of simulation results. The optimal value of residual stress depends on the type of contact (normal or sliding), coefficient of friction, and layer deformation mode (i.e., plastic deformation or cracking).

1. Introduction

Residual stress due to manufacturing process exists in surfaces of many engineering applications. Surface property modification technique can generate residual stress, tensile stress during surface thermal quenching, and compressive stress resulting from shot peening and ion implantation. The importance of residual stress during thin-film deposition has become more and more significant as thin film media are widely used in integrated circuits, MEMS, and wear protection coatings on cutting tools or hard disks in computers. Both experimental and theoretical studies have been carried out to determine the origin and magnitude of residual stress and its effect on film properties and mechanical performance.

The presence of residual stress in thin films has been the focus of many experimental investigations, and several techniques have been developed to measure residual stress in thin films deposited on substrates. Nix (1989) summarized the common experimental techniques used to measure stresses in thin films including X-ray diffraction, optical interferometry, and laser scanning. Mehregany et al. (1997) determined the tensile residual stress in 3C-SiC films from load-deflection measurements of suspended diaphragms. Kamiya et al. (1999) evaluated the residual stress distribution in thin diamond films deposited on Si substrate by measuring the curvature and with the aid of Raman spectroscopy. The average intrinsic stress was found to be tensile, although a high compressive stress was observed in a very small region near the film/substrate interface. Lu and Komvopoulos (2000) proposed a technique for evaluating residual stresses in ultrathin films by using small amounts of Ar atoms implanted in the film as stress-sensing probes. This technique is especially useful when the film is only a few nanometers thick, where conventional techniques may not be suitable.

Machlin (1995) reviewed the various theories proposed to explain the intrinsic stresses

that have been found in thin films. Most of the stresses in thin films exist because the film is bonded to a massive substrate. Thus, any change in length along the film plane (either due to thermal mismatch or lattice mismatch), which is not matched exactly by an equal change in length in the substrate, will result in a stress in the film. During non-energetic deposition of metal films, intrinsic stresses are usually tensile and their magnitudes can equal or exceed the yield strength values for the severely cold-worked state (Pulker, 1982, Martinez and Abermann, 1982, Abermann and Koch, 1980). This result may be explained on the basis that the yield strength in thin films exceeds that for bulk material for comparable conditions of dislocation density and grain size. A compressive intrinsic stress is found in films produced from condensation of energetic particles or grown under energetic particle bombardment. The maximum value of the compressive stress is again the yield strength, but in compression.

Serving as a wear protection overcoat is one of the most important applications of thin film. Therefore, experimental studies have been conducted to understand the correlation between residual stress and tribological performance of thin film. Kao et al. (1989) investigated the mechanical and tribological characteristics of thin chromium oxide films by controlling the process parameters in reactive deposition and subsequent annealing. Their experimental results demonstrated that wear resistance was reduced by tensile residual stress, but was increased by a moderate compressive residual stress. Mounier et al. (1995), Mounier and Pauleau (1997) carried out ball-on-disk tribological tests on amorphous carbon films deposited by sputtering. The residual stresses in the films deposited on Si substrates were obtained from the change in the radius of curvature of substrates measured before and after deposition of films and the residual stresses were found to be compressive. They attribute severe damage and formation of a large quantity of wear debris in the wear tracks to high level of compressive residual stresses in a-C

films. They further suggested that the residual stress level might affect the mechanical resistance and integrity of the deposited material, i.e., brittleness, fracture resistance or fragility, and also the adherence of a-C films to various substrates. A high level of tensile stresses can produce film and substrate cracking whereas excessive compressive stresses can lead to delamination of films from the substrate surface and formation of blister zone. Scharf and Barnard (1997) studied the wear and frictional behavior of ultrathin (25 nm) a:SiC/SiC-N overcoat using a depth sensing nanoindentation multiple sliding technique. They found that the presence of compressive residual stress improved the wear resistance for the SiC-N film. The improvement was attributed to the facts that compressive stress can close through thickness cracks and densify the microstructure. Herr and Broszeit (1997) investigated the effect of annealing process on the tribological properties of sputtered titanium, hafnium and chromium based nitride and boride layers on steel and titanium alloy substrate. The microhardness test results showed that hardness is higher in films with higher compressive residual stress. However, high compressive stresses also resulted in premature failures during scratch test, which was proved by cracking and spalling at low critical loads. Kato et al. (1999) measured change in curvature of silicon substrates to detect internal stress in CN_x coating. Their wear tests showed that internal compressive stress reduced wear within the range of stress in their study. They suggested that a thin coating, after optimizing synthesis routine and processing conditions, may have a longer wear life if it has a suitable internal stress. Zhong et al. (2001) investigated the mechanical properties and tribological performance of the sputtered Ti-B-C-N films. Varying magnitudes of compressive residual stresses were found in films deposited at different substrate bias and with different argon-nitrogen atmospheres. The wear resistance was found to be inversely related to the compressive residual stress in the film measured using X-ray diffraction analysis.

Analytical and numerical approaches have also been applied to study residual stress effect. Hills and Ashelby (1982) determined and compared the elastic and shakedown limits for elastic homogeneous half space under sliding containing a cylindrical residual stress system using analytical solution given by Hamilton and Goodman (1966). The optimum value of compressive residual stress was found for different coefficient of friction. In their study, residual stress was assumed to be a constant along the depth direction of homogeneous half space. Mesarovic and Fleck (1999) performed finite element simulation to evaluate the role of residual stress within the elastic-ideally plastic half-space under spherical indentation. Indentation predictions are shown for the cases of vanishing pre-stress, equibiaxial tension of magnitude $\mathbf{s}_Y/2$ and equibiaxial compression of magnitude $-\mathbf{s}_Y/2$, where \mathbf{s}_Y is the yield strength. For both the similarity regime and the finite-deformation plasticity regime of indentation, residual stress has a negligible effect on the average contact pressure, on the normalized contact area, and on the contact stiffness. However, within the elastic-plastic indentation regime, the average contact pressure and normalized contact area decrease with increasing residual tension, while the contact stiffness is approximately independent of the initial stress state. While the overall plastic zone shape depends upon the level of pre-stress, the region of large strain (effective strain greater than 0.01) is practically identical in all three cases of pre-stress. Thus, pre-stress only has an effect in the vicinity of the elastic-plastic boundary, where elastic and plastic strains are of similar magnitude. Finite element method has been recently used to by Bai et al. (2000) to study the effect of internal stress on mechanical properties of thin films. The results of their simulation showed that the film with compressive internal stress has larger hardness and modulus than that without compressive internal stress; and vice versa if the internal stress is tensile.

It can be seen from the aforesaid studies that most of them are experimental, although

they provided invaluable insight into the understanding of residual stress effect on tribological performance and mechanical properties of thin film, there is still a lack of a overall picture, as few theoretical studies were able to include layered media, elastic-plastic constitutive relationship, normal/sliding contact, and wide range of top layer internal stress. However, these aspects are key to promote understanding of internal stress effect on thin film used as tribological application, which is the main objective of this study. In order to achieve this, a three-dimensional finite element model was developed, and its accuracy was validated by favorable comparisons of simulation result with analytical solutions from previous study. Finite element results for the stresses, and plastic strain in an elastic-plastic layered medium under normal and sliding contact are presented for different magnitudes of internal stress and coefficient of friction. The significance of internal stress and coefficient of friction the likelihood of the layered medium to undergo yielding and cracking are interpreted in the context of simulation results.

2. Finite Element Model

In the finite element model the spherical asperity was assumed to be rigid and the layered medium was modeled by three-dimensional, eight-node, linear hexahedron finite elements. In order to save the computation time only one-half of the sphere and the medium were modeled facilitated by the symmetric nature of the problem. The cross section at the symmetry plane $x = 0$ of the three-dimensional mesh of the finite element model is shown in Figure 1. The layered medium is discretized using 11,113 elements with a total of 15,006 nodes. To obtain accurate stress/strain field the mesh is refined in the region near the asperity as it indents in the negative y direction, and then slides along the positive z -direction. The x , y , z dimensions of the mesh

normalized by the radius R of the rigid spherical asperity are 1, 0.976, and 3. The boundary conditions are as follows: the nodes on planes $x/R = 0$ and 1 were fixed against displacement in the x -direction, the nodes on plane $y/R = -0.976$ were fixed against displacement in the y -direction, and the nodes on planes $z/R = -1$ and 2 were fixed against displacement in the z -direction. The layered medium consists of a layer of thickness and a substrate, whose thickness and physical properties are given in Table 1. These data are typical of carbon overcoats and magnetic layers used in hard disks.

The interaction between the deformable layered medium and the rigid sphere is modeled with finite-sliding formulation using contact elements. At each integration point these elements construct a measure of overclosure (interpenetration of the surfaces) and measures of relative shear sliding. These kinematic measures are then used, together with appropriate Lagrange multiplier techniques, to determine surface interactions: contact and friction.

The constitutive model of the normal interaction between the surfaces is defined as:

$$p = 0, \quad \text{for } \mathbf{d} < 0, \quad (\text{no contact}) \quad (1a)$$

$$p = K \mathbf{d}, \quad \text{for } \mathbf{d} \geq 0, \quad (\text{contact}) \quad (1b)$$

where p is the contact pressure between two surfaces at a point, \mathbf{d} is the overclosure of the surfaces K is the stiffness in stick, determined through an iterative procedure that satisfies equilibrium. The model given by Eq. (1) indicates that when the clearance between two surfaces reduces to zero, separated surfaces come into contact and the contact pressure assumes a nonzero value, which depends on the material properties and boundary conditions. When the two surfaces separate, the contact pressure reduces to zero.

Coulomb friction model is applied as the constitutive model of the sliding interaction to the surfaces. No relative motion or stick occurs if the shear stress \mathbf{t} is less than the critical stress,

t_{crit} , which is proportional to the contact pressure, p , in the form $t_{crit} = f p$, where f is the coefficient of friction. No relative motion is actually approximated by stiff elastic behavior. The stiffness is chosen such that the relative motion from the position of zero shear stress is bounded by the allowable maximum elastic slip, 0.5% of the average length of all contact elements in the model. If the shear stress is at the critical stress, macroscopic lateral movement or slip can occur. Thus, the stick and slip conditions at the contact interface can be expressed as

$$t < fp \quad (\text{stick}) \quad (2a)$$

$$t = fp \quad (\text{slip}) \quad (2b)$$

Two values of coefficient of friction, 0.25 and 0.5, were specified to the contact elements in simulation cases.

When residual stress \mathbf{s}_r was introduced to the top layer, the stress state may not be an exact equilibrium state for the finite element model. Therefore, an initial step was included to allow ABAQUS to check for equilibrium and iterate, if necessary, to achieve equilibrium. Eight different magnitudes of \mathbf{s}_r were used and \mathbf{s}_r varied from -0.75 to $+0.95$ times the yield strength of the layer.

The constitutive relationship of both layer and substrate materials is assumed to be elastic-perfectly plastic, following yield criterion

$$\mathbf{s}_M = \sqrt{\frac{3}{2} S_{ij} S_{ij}} = \mathbf{s}_Y, \quad (3)$$

where \mathbf{s}_M is the von Mises equivalent stress, S_{ij} is the deviatoric stress tensor ($S_{ij} = \mathbf{s}_{ij} - \mathbf{s}_{kk} \mathbf{d}_{ij} / 3$, where \mathbf{s}_{ij} is the stress tensor and \mathbf{d}_{ij} is Kronecker's delta function), and \mathbf{s}_Y is the yield strength in uniaxial tension.

Two types of quasi-static simulations were performed with the multi-purpose finite element code ABAQUS: (a) normal contact involving indentation and unloading, and (b) sliding contact consisting of indentation, sliding, and unloading. Indentation of the layered medium by the asperity to a depth corresponding to a fixed normal load was modeled in one step of 21 to 24 increments each. Unloading was simulated in one step of 6 to 11 increments each. Sliding simulations comprised five incremental displacements $Dz/R = 0.05, 0.15, 0.35, 0.65, \text{ and } 0.95$ of the asperity under the given load in the z direction each having 11-19 increments. The typical computational time on a Pentium III 550 workstation was about 20,000 to 49,000 CPU seconds.

3. Model Validation

To examine the accuracy of the finite element model, a normal contact simulation was performed for an elastic homogeneous half-space indented by a rigid sphere. Figure 2 shows the variations of the von Mises equivalent stress and first principal stress at the surface along the z -direction ($x = y = 0$) predicted by the finite element model and the analytical solution of Huber (1904). The stresses are normalized by the maximum contact pressure p_0 and coordinate z by the contact radius r . The good agreement between the two methods indicates the validity of the finite element model and the correctness of the assumed boundary conditions for contact analysis.

4. Results and Discussions

A series of finite element simulations were performed with varying magnitudes of residual stress and coefficient of friction. Finite element simulation results are presented to illustrate the effect of residual stress and coefficient of friction on the stress and strain fields. Results from sliding simulation are given for $Dz/R = 0.95$. The locations of maximum stress and strain in the layered medium are listed in Tables 2 to 4.

To provide a general guideline to the FEM simulation, analytical approach was first applied to evaluate the effect of residual stress on subsurface stress field of elastic homogeneous half-space under normal Hertzian contact. As will be shown later, there are some similarities between the results for a homogeneous medium and a layered medium. Varying magnitudes of equibiaxial residual stress (in the x and z directions) were superimposed to the normal contact stress field obtained from Huber's analysis (Huber, 1904). A MATLAB code was written to find the maximum von Mises stress and solve the eigenvalue problem to obtain the maximum first principal stress under different magnitudes of equibiaxial residual stress. Poisson ratio was assumed to be 0.3 and the result is plotted in Figure 3. To minimize von Mises stress, residual stress needs to be $-0.22p_0$, where p_0 is the peak contact pressure. Maximum first principal stress is suppressed to zero when residual stress is equal or smaller than $-0.13p_0$. It is noticed that when residual stress is zero the maximum first principal stress is $0.13p_0$. This is not a coincidence, because the maximum first principal stress lies in the same direction as that of the residual stress, and a compressive residual stress can cancel out the tensile stress induced by indentation. Therefore, for elastic homogeneous half-space under normal Hertzian contact, the optimal equibiaxial residual stress is $-0.22p_0$ to minimize the possibilities of yielding and crack initiation.

The results of FEM simulation of layered medium under normal and sliding contact with rigid sphere are displayed in Figures 4 to 9. Figure 4 through 6 are results in the layer.

Figure 4 shows the dependence of maximum von Mises stress in the layer on residual stress during indentation, sliding, and unloading. During indentation, similar to the analytical result of homogeneous half space, there is an optimal value of compressive residual stress to minimize the maximum von Mises stress and the value is between $-0.25p_0$ and $-0.5p_0$. The effect of friction is negligible for indentation. During unloading after indentation, sliding at $f = 0.25$,

and unloading after sliding at $f = 0.25$, the von Mises stress is minimum for residual stress close to zero. However, the residual stress does not affect the maximum von Mises stress during sliding at $f = 0.5$ and the subsequent unloading. This is actually because yielding occurs in the layer at higher friction, and the maximum von Mises stress cannot increase beyond yield strength even under larger residual stress. The effect of coefficient of friction is insignificant during indentation and subsequent unloading, mainly because of the limited relative slippage between the contacting surfaces. During sliding, the higher coefficient of friction is expected to lead to higher von Mises stress; however, it is noticed that at high magnitudes of residual stress (either tensile or compressive) there is no difference between the value of maximum von Mises stress for $f = 0.25$ and 0.5 . This is also due to yielding in the layer under larger residual stress during sliding.

To better illustrate the effect of residual stress and coefficient of friction during sliding after yielding occurs, the maximum equivalent plastic strain in the layer varying with the magnitude of residual stress is shown in Figure 5. No re-yielding occurs during the subsequent unloading after sliding. It is shown that neither compressive nor tensile residual stress reduces the plastic strain in the layer material. So, from maximum plastic strain point of view, the optimal residual stress is zero, or smaller than $|0.5p_0|$ for $f = 0.25$. Higher coefficient of friction generates higher plastic strain and the increase at a given residual stress is approximately the same. The location of the maximum equivalent plastic strain during sliding was found to be at the surface of the layer for tensile residual stress, and at the layer/substrate interface for zero or compressive residual stress.

The dependence of the maximum first principal stress in the layer on residual stress is shown in Figure 6. Maximum first principal stress is considered to be responsible for crack initiation especially in a brittle material. After unloading following indentation, the maximum

first principal stress remains approximately the same (Fig. 6(a)). This is caused by the development of plasticity mainly in the substrate, and after unloading the plastic zone places a constraint to the surrounding elastic region. The overall trend during indentation closely resembles that of the analytical result (Fig. 3), however, the compressive stress required to suppress the maximum first principal stress increases to around $-0.4p_0$, which is needed to cancel out the maximum first principal stress at residual stress equal to zero. It is noticed that this magnitude is higher than that in homogeneous half space ($0.13p_0$). This is because of the effect of lower Young's modulus and strength of the substrate. The more compliant and plastically deformed substrate cannot provide a strong support to the layer; therefore, the layer deforms more than if it was supported by a stronger material like itself, and hence encounters higher stress. It is the larger elastic and plastic deformation in the substrate that causes the increase of the maximum first principal stress in the layer. When sliding occurs, for $f = 0.25$, the residual stress has to increase to $-p_0$ to suppress the maximum first principal stress close to zero. This increase is caused by the added shear stress component during sliding. For $f = 0.5$, increasing the residual stress cannot suppress the maximum first principal stress in the layer to zero any more. This is caused by the larger plastic deformation in the substrate, which can be seen from the location of maximum first principal stress. During sliding, the maximum first principal stress location is always at the layer surface for $f = 0.25$, but for high level of compressive residual stress and $f = 0.5$, the maximum stress location shifts to the layer/substrate interface. During indentation, the maximum first principal stress is found to be at the layer surface for zero or tensile residual stress, and in the bulk of the layer for compressive residual stress. During unloading after indentation, the maximum first principal stress location is always the layer/substrate interface. The results shown in Figs. 5 and 6 demonstrate the important role of the

residual stress on the resistance against plastic deformation and cracking of layered media subjected to normal and sliding contact.

The stress and strain results in the substrate are shown in Figures 7 to 9.

Figure 7 shows the dependence of the maximum von Mises stress on the residual stress in the layer after unloading from indentation and sliding for $f = 0.25$ and 0.5 . It is noticed that after unloading from indentation there is an optimal “tensile” residual stress (around p_0) that minimizes the maximum von Mises stress. After unloading from sliding, the higher coefficient of friction raises the maximum von Mises stress, which is expected because of the larger plastic deformation occurring mainly in the substrate at higher coefficient of friction (as shown in Figure 8). Tensile is put in quotation marks because tensile residual stress in the layer is actually compressive in the substrate. With this in mind, Figs. 8 and 9 can also be easily understood. Upon unloading from indentation or sliding, for all magnitudes of residual stress, the maximum von Mises stress is located at the layer/substrate interface.

Figure 8 shows the maximum equivalent plastic strain versus the residual stress. Again, the coefficient of friction only affects the plastic strain during sliding. Higher coefficient of friction renders larger plastic strain and the increase amount is about the same at different magnitude of residual stress. During indentation and sliding with $f = 0.25$, a tensile residual stress in the layer of $\sim 1.5p_0$ minimizes the plastic deformation in the substrate. This trend is similar to that of as the maximum von Mises stress in homogeneous medium (Fig. 3) as tensile residual stress in the layer is balanced by a compressive stress in the substrate. Therefore, plastic deformation in the substrate is minimized by compressive stress in the substrate. During sliding, the maximum equivalent plastic strain is located at the interface between the layer and substrate for both $f = 0.25$ and 0.5 .

In Fig. 9 the maximum first principal stress is plotted as a function of the residual stress. The significance of coefficient of friction is only shown during sliding and the following unloading. It is noticed that \mathbf{s}_I^{max} is higher after unloading than during sliding. This is caused by the mismatch unloading of elastic and plastic regions in the substrate. Plastic zones are in both the layer and substrate. Also, elastic recovery is different in the layer and substrate ($E_l > E_s$). During sliding and the unloading afterwards, the maximum first principal stress is always located at the interface between the layer and substrate for both $f = 0.25$ and 0.5 .

To further illustrate the effect of friction and residual stress on plastic deformation, a comparison of plastic zones during sliding for different coefficient of friction and residual stress is shown in Fig. 10 to 13. The spherical sliding asperity starts from position 1 and stops at position 2. At a given coefficient of friction, increasing the magnitude of residual stress (either tensile or compressive) enlarges the plastic zone in the layer, although tensile stress has a more significant effect than compressive stress. However, the depth of the plastic zone in the substrate is increased by higher compressive stress in the layer (balancing tensile stress in the substrate). Higher coefficient of friction renders larger plastic zones in both the layer and substrate, more noticeably in the layer, which is apparently because the substrate is separated from the sliding asperity by the layer. It is also noticed that tensile (compressive) residual stress tends to induce larger plastic zone at the trailing (front) edge along the sliding direction. This can be explained by the fact that during sliding, the dominant stress generated by shear force at the trailing (front) edge is tensile (compressive). Therefore, tensile (compressive) residual stress helps enlarge plastic deformation at the trailing (front) edge.

5. Conclusions

A three-dimensional finite element analysis for normal & sliding contact of elastic-plastic layered media was performed in order to elucidate the role of the residual stress in the surface layer (overcoat) and coefficient of friction on the evolution of stress and strain fields. Based on the presented results and discussion, the following main conclusions can be drawn.

- (1) A three-dimensional finite element model for contact analysis was developed and validated by comparison of simulation results those obtained from an elastic normal contact analysis.
- (2) In the surface layer, the maximum first principal stress increases (decreases) with tensile (compressive) residual stress.
- (3) During indentation, the location of the maximum first principal stress in the layer shifts from the bulk to the surface of the layer as the residual stress changes from compressive to zero and tensile.
- (4) During indentation, the effect of coefficient of friction is negligible.
- (5) During sliding, the magnitude of optimal residual stress depends on the coefficient of friction. Higher coefficient of friction promotes plasticity and intensifies the maximum first principal stress in both the layer and substrate media.
- (6) During sliding, the location of maximum plastic strain in the substrate is always at the interface between the layer and substrate. The location of maximum plastic strain in the layer shifts from the interface between the layer and substrate to the surface of the layer as the residual stress changes from compressive to tensile.
- (7) During unloading, unmatched elastic relaxation between plastic and elastic regions in the substrate generates a higher maximum first principal stress than that during sliding.

- (8) During sliding and unloading, the location of the maximum first principal stress in the substrate is always at the interface between the layer and substrate.
- (9) The optimal value of normalized residual stress s_r/p_0 depends on the type of contact (normal or sliding), coefficient of friction, and deformation mode of the overcoat, i.e., plastic deformation or cracking.

Acknowledgments

This research was partially supported by the National Storage Industry Consortium (NSIC), Extremely High Density Recording (EHDR) Program, and the Computer Mechanics Laboratory at the University of California at Berkeley.

References

- Abermann, R., and Koch, R., 1980, "In situ determination of the structure of thin metal films by internal stress measurements: structure dependence of silver and copper films on oxygen pressure during deposition," *Thin Solid Films*, **66**, pp. 217- 232.
- Bai, M., Kato, K., Umehara, N., and Miyake, Y., 2000, "Nanoindentation and FEM Study of the Effect of INternal Stress on Micor/Nano Mechanical Property of Thin CN_x Films," *Thin Solid Films*, **377-378**, pp. 138-147.
- Hamilton, G. M., and Goodman, L. E., 1966, "The Stress Field Created by a Circular Sliding Contact," *Journal of Applied Mechanics*, **88**, pp. 371-378.
- Herr, W., and Broszeit, E., 1997, "Effect of an Annealing Process on the Tribological Properties of Sputtered Hard Coatings," *Surface and Coatings Technology*, **97**, pp. 669-674.
- Hills, D. A., and Ashelby, D. W., 1982, "The Influence of Residual Stresses on Contact-Load-Bearing Capacity," *Wear*, **75**, pp. 221-240.
- Huber, M. T., 1904, "Zur Theorie der Berührung Fester elastischer Körper," *Annalen der Physik*, **14**, pp. 153-163.

- Kato, K., Bai, M., Umehara, N., and Miyake, Y., 1999, "Effect of Internal Stress of CN_x coating on its Wear in Sliding Friction," *Surface and Coatings Technology*, **113**, pp. 233-241.
- Kamiya, S., Sato, M., and Saka, M., 1999, "Residual Stress Distribution in the Direction of the Film Normal in Thin Diamond Films," *Journal of Applied Physics*, **86**, pp. 224-229.
- Lu, W., and Komvopoulos, K., 2000, "Implanted Argon Atoms as Sensing Probes of Residual Stress in Ultrathin Films," *Applied Physics Letters*, **76**, pp. 3206-3208.
- Machlin, E. S., 1995, *Materials Science in Microelectronics, The Relationships between Thin Film Processing and Structure*, Giro Press, Croton-on-Hudson, NY.
- Martinez, H. P., and Abermann, R., 1982, "Interaction of O₂, CO, H₂O, H₂ and N₂ with thin chromium films studied by internal stress measurements," *Thin Solid Films*, **89**, pp. 133-138.
- Mehregany, M., Tong, L., Matus, L. G., and Larkin, D. J., 1997, "Internal Stress and Elastic Modulus Measurements on Micromachined 3C-SiC Thin Films," *IEEE Transactions on Electron Devices*, **44**, pp. 74-79.
- Mesarovic, S. Dj., and Fleck, N. A., 1999, "Spherical Indentation of Elastic-Plastic Solids," *Proceedings of the Royal Society (London), Series A*, **455**, pp. 2707-2728.
- Mounier, E., Juliet, P., Quesnel, E., and Pauleau, Y., 1995, "Dependence of Tribological Properties on Deposition Parameters for Nonhydrogenated Amorphous Carbon Films Produced by Magnetron Sputtering," *Surface and Coating Technology*, **77**, pp. 548-552.
- Mounier, E., and Pauleau, Y., 1997, "Mechanisms of Intrinsic Stress Generation in Amorphous Carbon Thin Films Prepared by Magnetron Sputtering," *Diamond and Related Materials*, **6**, pp. 1182-1191.
- Nix, W. D., 1989, "Mechanical Properties of Thin Films," *Metallurgical Transactions A*, **20A**, pp. 1989-2217.
- Pulker, H. K., 1982, "Mechanical properties of optical films," *Thin Solid Films*, **89**, pp. 191-204.
- Scharf, T. W., and Barnard, J. A., 1997, "Nanotribology of Ultrathin a:SiC/SiC-N overcoats using a depth sensing nanoindentation multiple sliding technique," *Thin Solid Films*, **308-309**,

pp. 340-344.

Zhong, D., Sutter, E., Moore, J. J., Mustoe, G. G. W., Levashov, E. A., and Disam, J., 2001, "Mechanical Properties of Ti-B-C-N Coatings Deposited by Magnetron Sputtering," *Thin Solid Films*, **398-399**, pp. 320-325.

Table 1. Thickness and properties of layer and substrate media of the finite element model

Medium	Layer	Substrate
Thickness, h/R	0.02	0.956
Elastic modulus, E (GPa)	168	130
Poisson ratio, ν	0.3	0.3
Yield strength, s_Y (GPa)	13	2.67

Table 2. Location of maximum von Mises stress s_M^{max}

Material	Step	COF	s_i/p_0							
			-1.60	-1.04	-0.51	0.00	0.49	0.95	1.43	1.88
Layer	indentation	0.25	I	I	I	I	I	I	N/A	N/A
		0.5	I	I	I	I	I	I	N/A	N/A
	unloading	0.25	I	I	I	I	I	I	I	S
		0.5	I	I	I	I	I	I	S	S
	sliding	0.25	N/A	N/A	I	S	S	N/A	N/A	N/A
		0.5	N/A	N/A	N/A	N/A	N/A	N/A	N/A	N/A
	unloading	0.25	S	I	I	I	I	I	S	S
		0.5	S	I	I	I	I	I	S	S
Substrate	indentation	0.25	N/A	N/A	N/A	N/A	N/A	N/A	N/A	N/A
		0.5	N/A	N/A	N/A	N/A	N/A	N/A	N/A	N/A
	unloading	0.25	I	I	I	I	I	I	I	I
		0.5	I	I	I	I	I	I	I	I
	sliding	0.25	N/A	N/A	N/A	N/A	N/A	N/A	N/A	N/A
		0.5	N/A	N/A	N/A	N/A	N/A	N/A	N/A	N/A
	unloading	0.25	I	I	I	I	I	I	I	I
		0.5	I	I	I	I	I	I	I	I

I: layer/substrate interface, S: layer surface, N/A: yielding has occurred, multiple points have reached yield strength

Table 3. Location of maximum equivalent plastic strain e_p^{max}

Material	Step	COF	s_i/p_0							
			-1.60	-1.04	-0.51	0.00	0.49	0.95	1.43	1.88
Layer	indentation	0.25	N/A	N/A	N/A	N/A	N/A	N/A	I	I
		0.5	N/A	N/A	N/A	N/A	N/A	N/A	I	I
	unloading	0.25	N/A	N/A	N/A	N/A	N/A	N/A	I	I
		0.5	N/A	N/A	N/A	N/A	N/A	N/A	I	I
	sliding	0.25	I	I	N/A	N/A	S	S	S	S
		0.5	I	I	I	I	S	S	S	S
	unloading	0.25	I	I	N/A	N/A	S	S	S	S
		0.5	I	I	I	I	S	S	S	S
Substrate	indentation	0.25	B	B	B	B	B	B	I	I
		0.5	I	I	I	B	B	B	I	I
	unloading	0.25	B	B	B	B	B	B	I	I
		0.5	I	I	I	B	B	B	I	I
	sliding	0.25	I	I	I	I	I	I	I	I
		0.5	I	I	I	I	I	I	I	I
	unloading	0.25	I	I	I	I	I	I	I	I
		0.5	I	I	I	I	I	I	I	I

N/A: yielding has not occurred,

Table 4. Location of maximum first principal stress s_I^{max}

Material	Step	COF	s_i/p_0							
			-1.60	-1.04	-0.51	0.00	0.49	0.95	1.43	1.88
Layer	indentation	0.25	B	B	B	S	S	S	S	S
		0.5	B	B	B	S	S	S	S	S
	unloading	0.25	I	I	I	I	I	I	I	I
		0.5	I	I	I	I	I	I	I	I
	sliding	0.25	S	S	S	S	S	S	S	S
		0.5	I	I	S	S	S	S	S	S
	unloading	0.25	S	I	I	I	I	I	I	S
		0.5	I	I	I	I	I	I	S	S
Substrate	indentation	0.25	I	I	I	B	B	I	I	I
		0.5	I	I	I	B	B	I	I	I
	unloading	0.25	I	I	I	B	I	I	I	I
		0.5	I	I	I	I	I	I	I	I
	sliding	0.25	I	I	I	I	I	I	I	I
		0.5	I	I	I	I	I	I	I	I
	unloading	0.25	I	I	I	I	I	I	I	I
		0.5	I	I	I	I	I	I	I	I

B: bulk of layer or substrate,

List of Figures

- Fig. 1 Cross section ($x = 0$) of three-dimensional finite element mesh used in the normal/sliding contact simulations and a detail view of the mesh near the surface.
- Fig. 2 Comparison of finite element and analytical results for (a) von Mises stress and (b) first principal stress at the surface of on an elastic homogeneous medium indented by a rigid sphere.
- Fig. 3 Maximum von Mises equivalent stress and maximum first principal stress versus residual stress in an elastic homogeneous half-space subjected to Hertzian normal traction.
- Fig. 4 Maximum von Mises equivalent stress in the layer of an elastic-plastic layered medium in contact with a rigid sphere versus residual stress for $f = 0.25$ and 0.5 : (a) indentation and unloading, and (b) sliding and unloading.
- Fig. 5 Maximum equivalent plastic strain in the layer of an elastic-plastic layered medium in sliding contact with a rigid sphere versus residual stress for $f = 0.25$ and 0.5 .
- Fig. 6 Maximum first principal stress in the layer of an elastic-plastic layered medium in contact with a rigid sphere versus residual stress for $f = 0.25$ and 0.5 : (a) indentation and unloading, and (b) sliding and unloading.
- Fig. 7 Maximum von Mises equivalent stress in the substrate of an elastic-plastic layered medium in contact with a rigid sphere versus residual stress after unloading from indentation and sliding for $f = 0.25$ and 0.5 .
- Fig. 8 Maximum equivalent plastic strain in the substrate of an elastic-plastic layered medium in contact with a rigid sphere versus residual stress for $f = 0.25$ and 0.5 : (a) indentation, and (b) sliding.

Fig. 9 Maximum first principal stress in the substrate of an elastic-plastic layered medium in contact with a rigid sphere versus residual stress for $f = 0.25$ and 0.5 : (a) indentation and unloading, and (b) sliding and unloading.

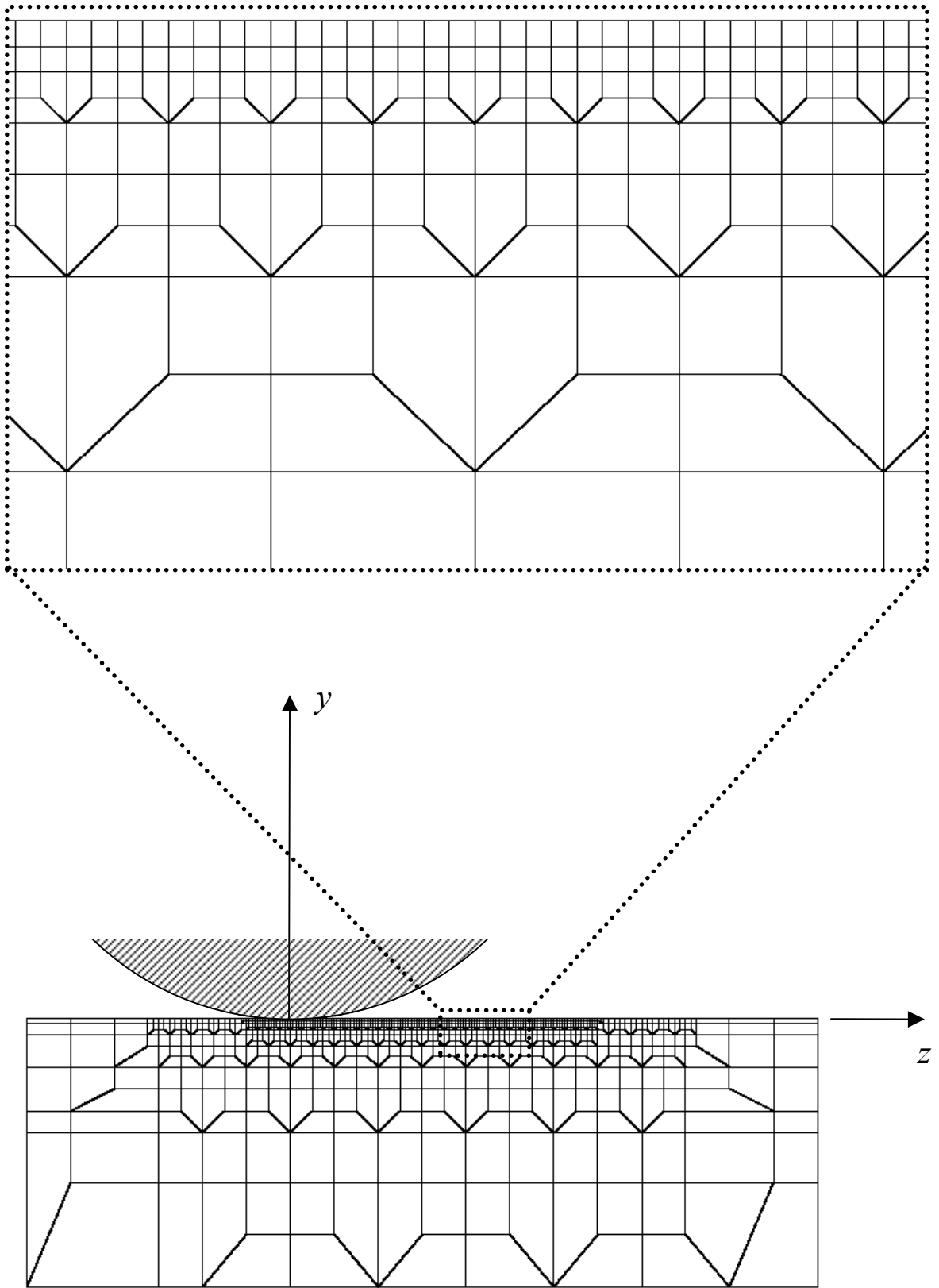


Figure 1

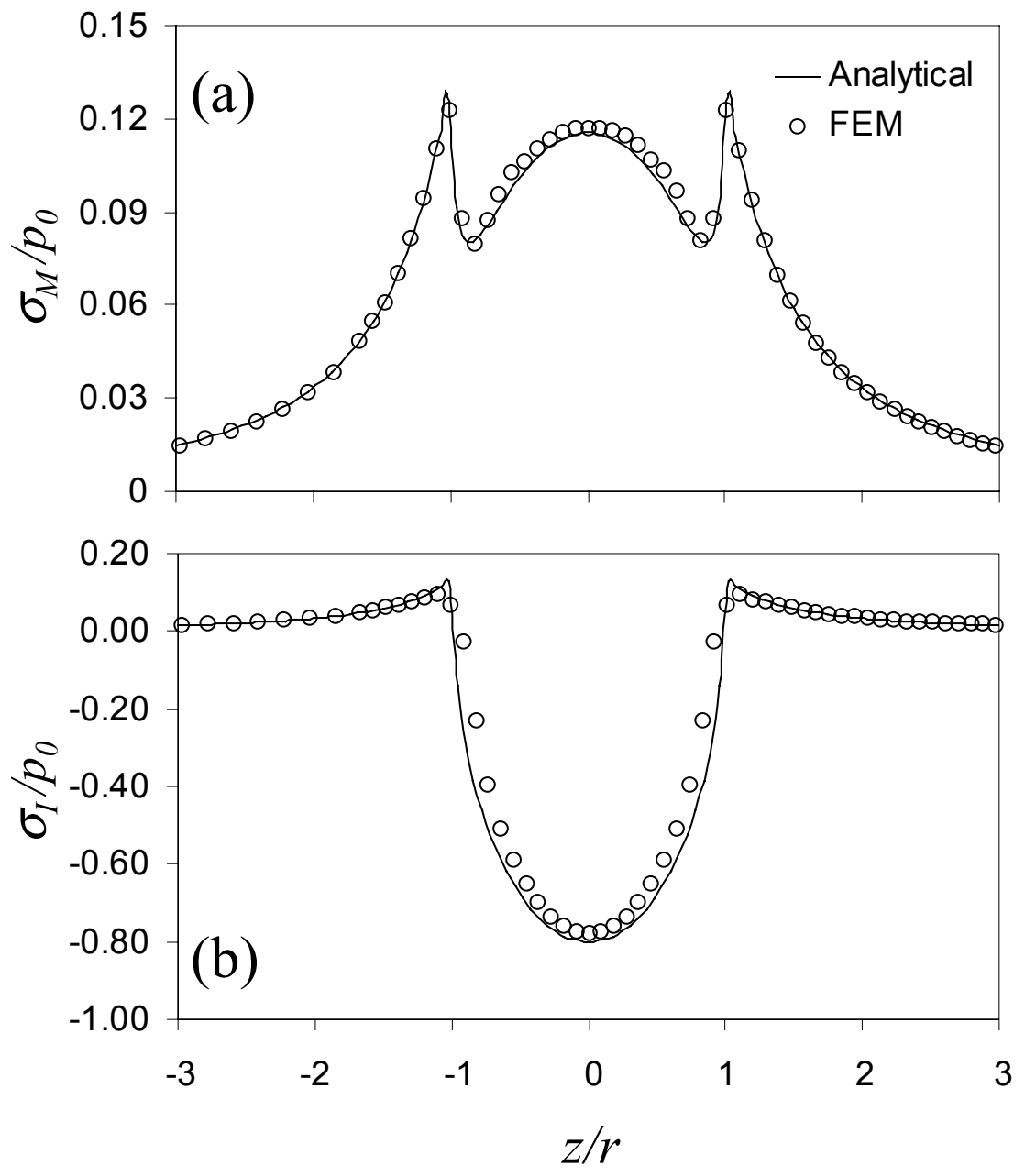


Figure 2

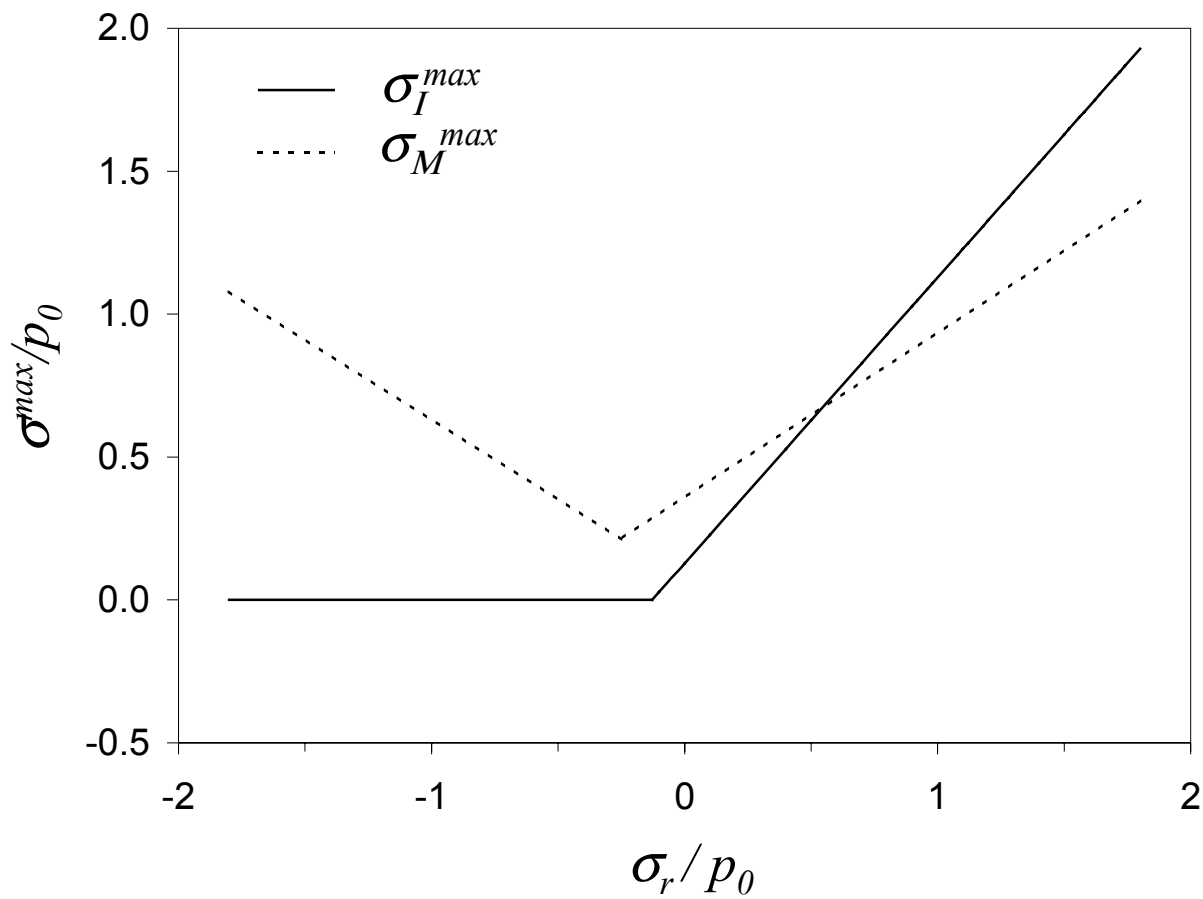


Figure 3

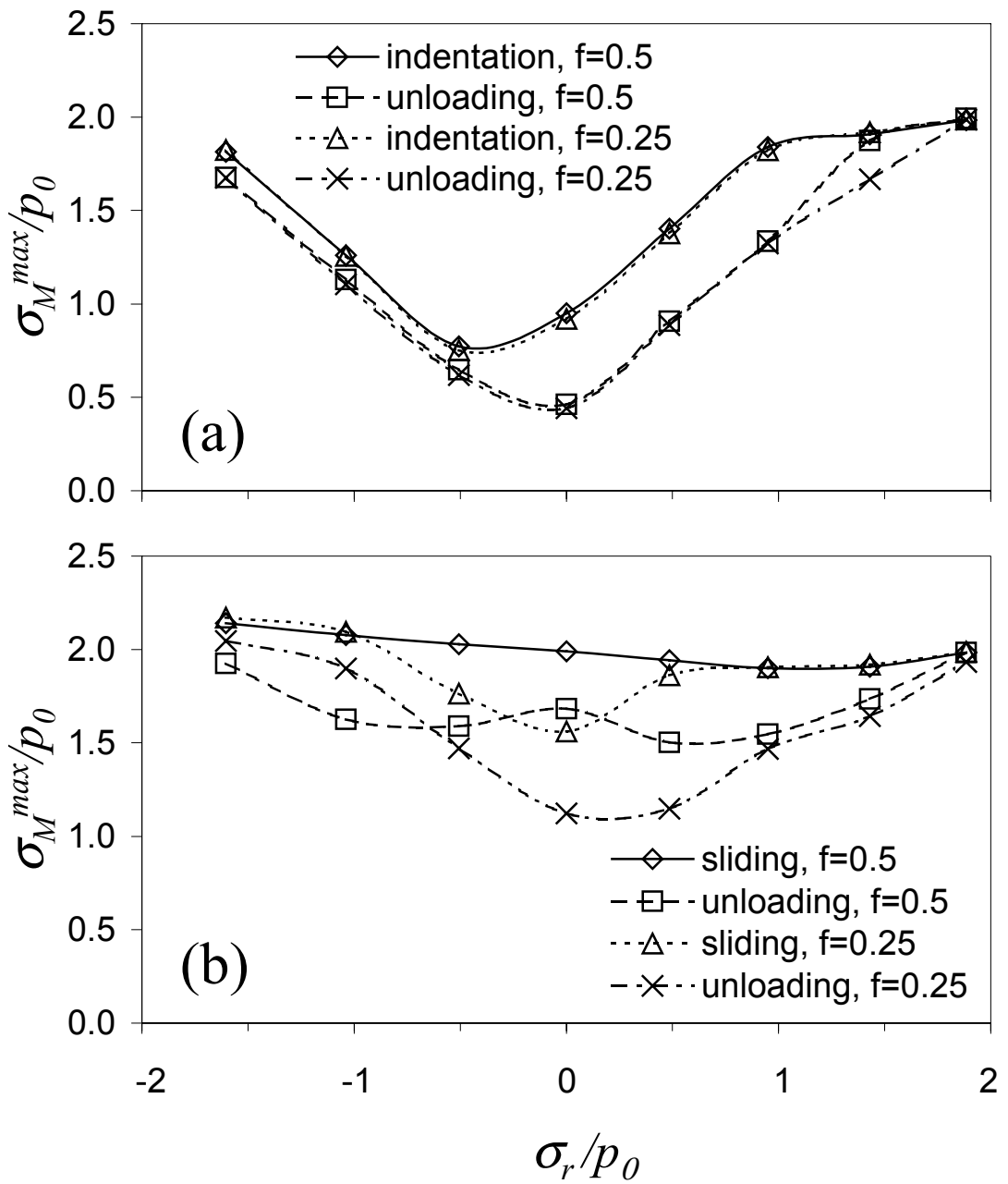


Figure 4

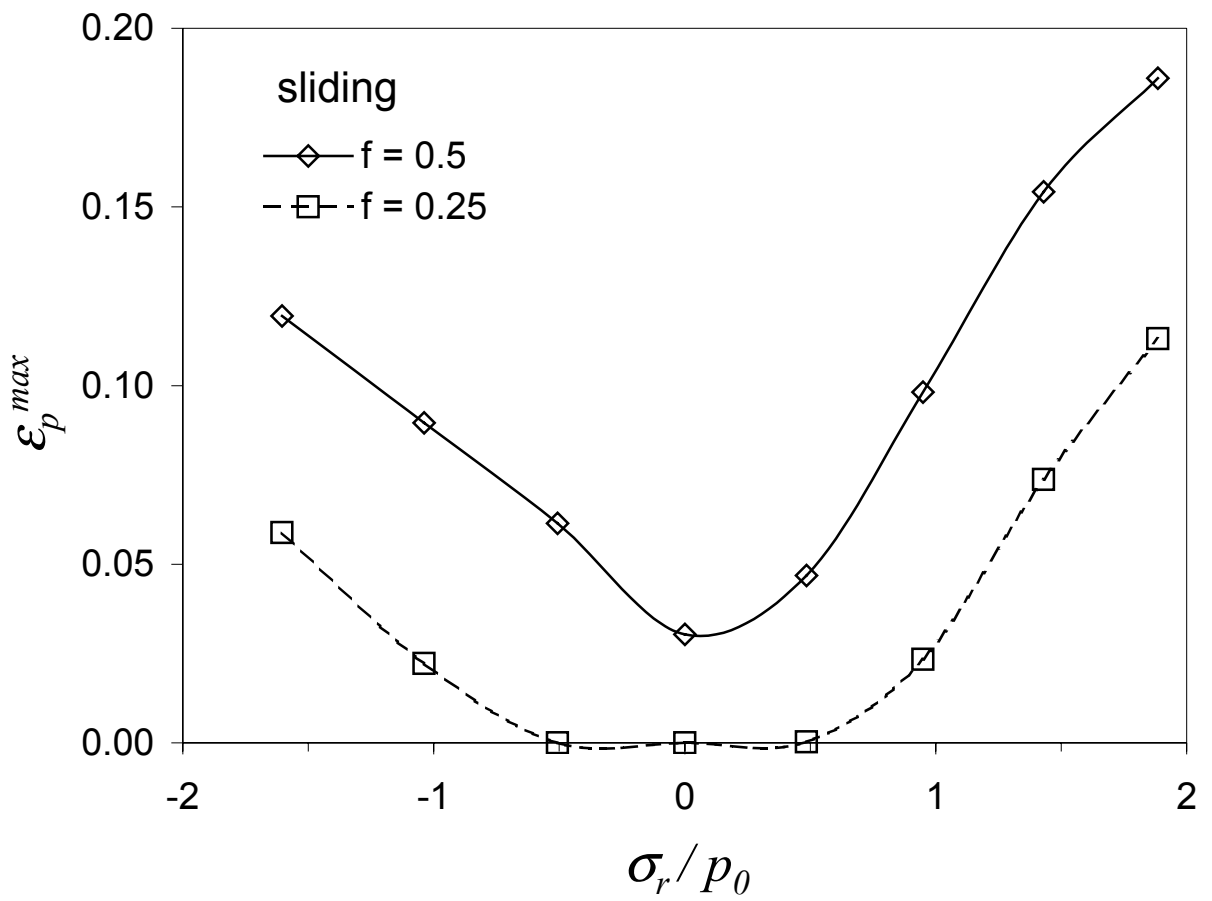


Figure 5

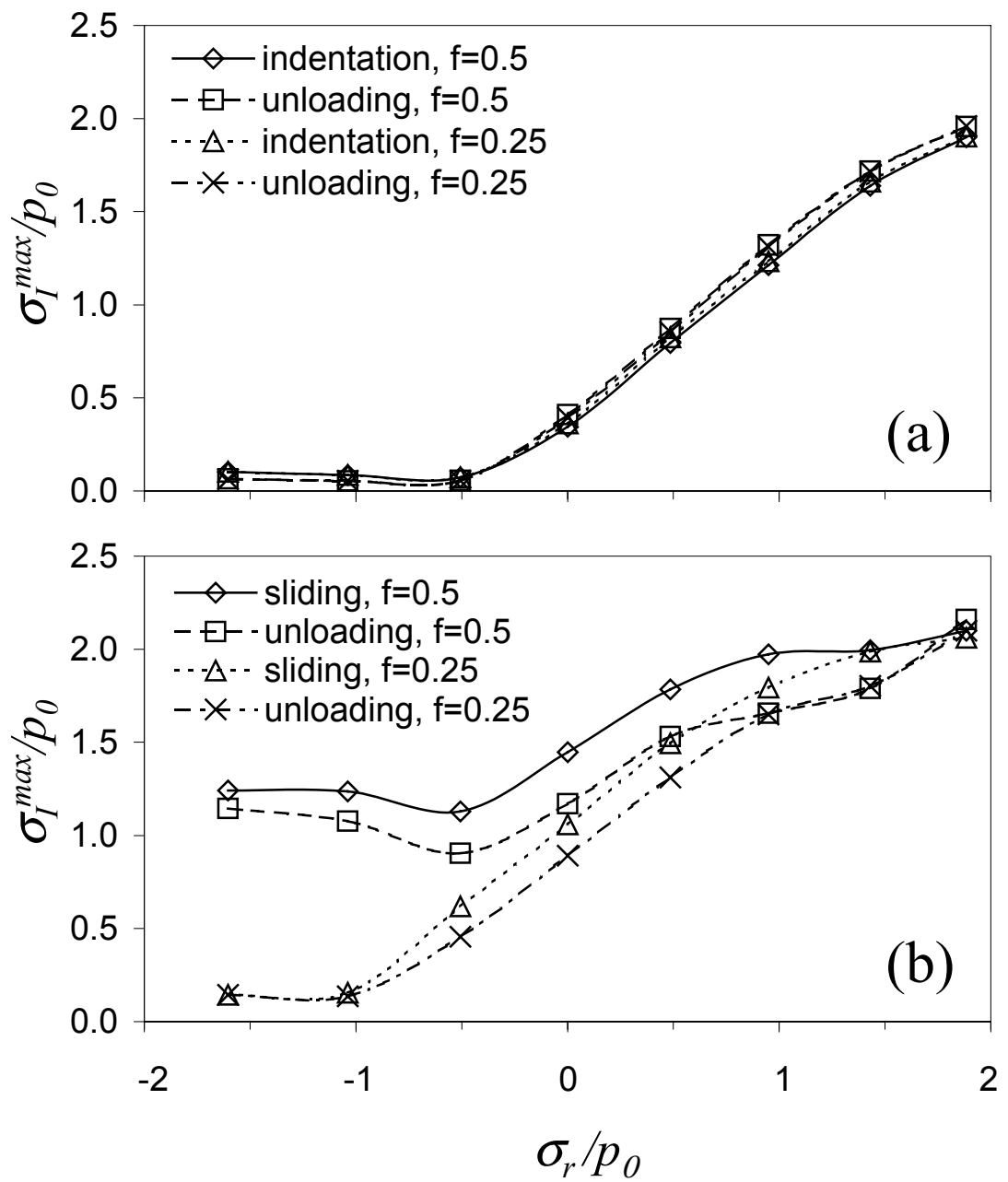


Figure 6

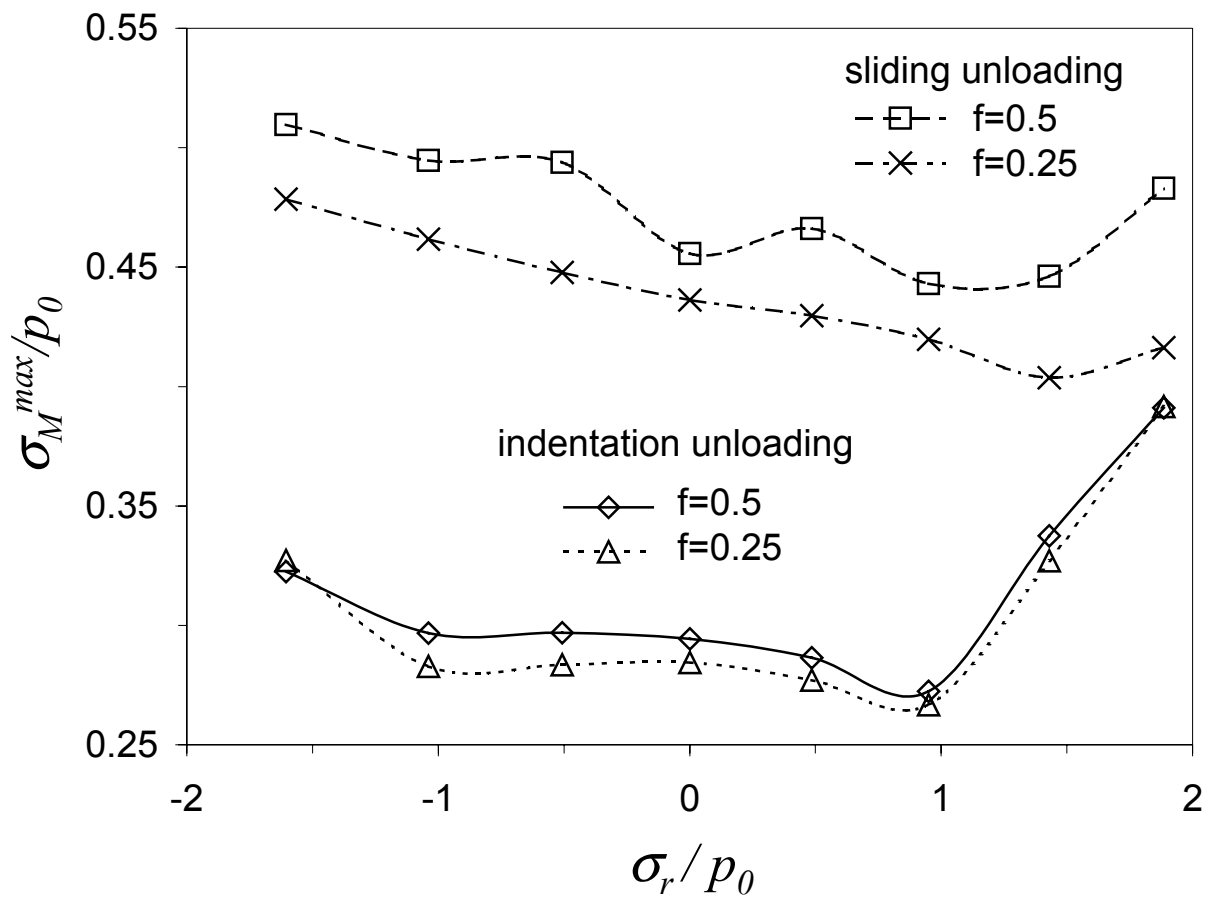


Figure 7

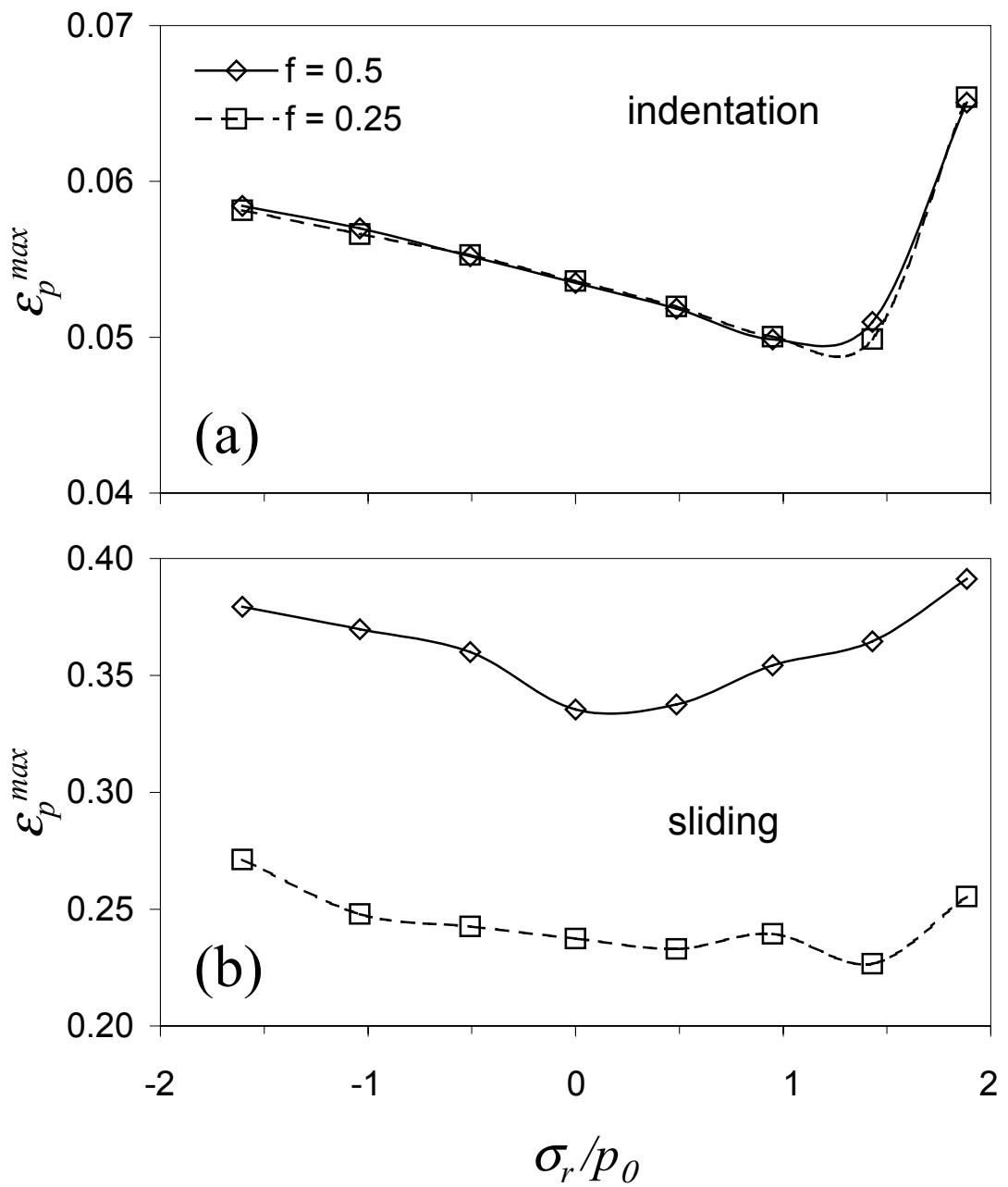


Figure 8

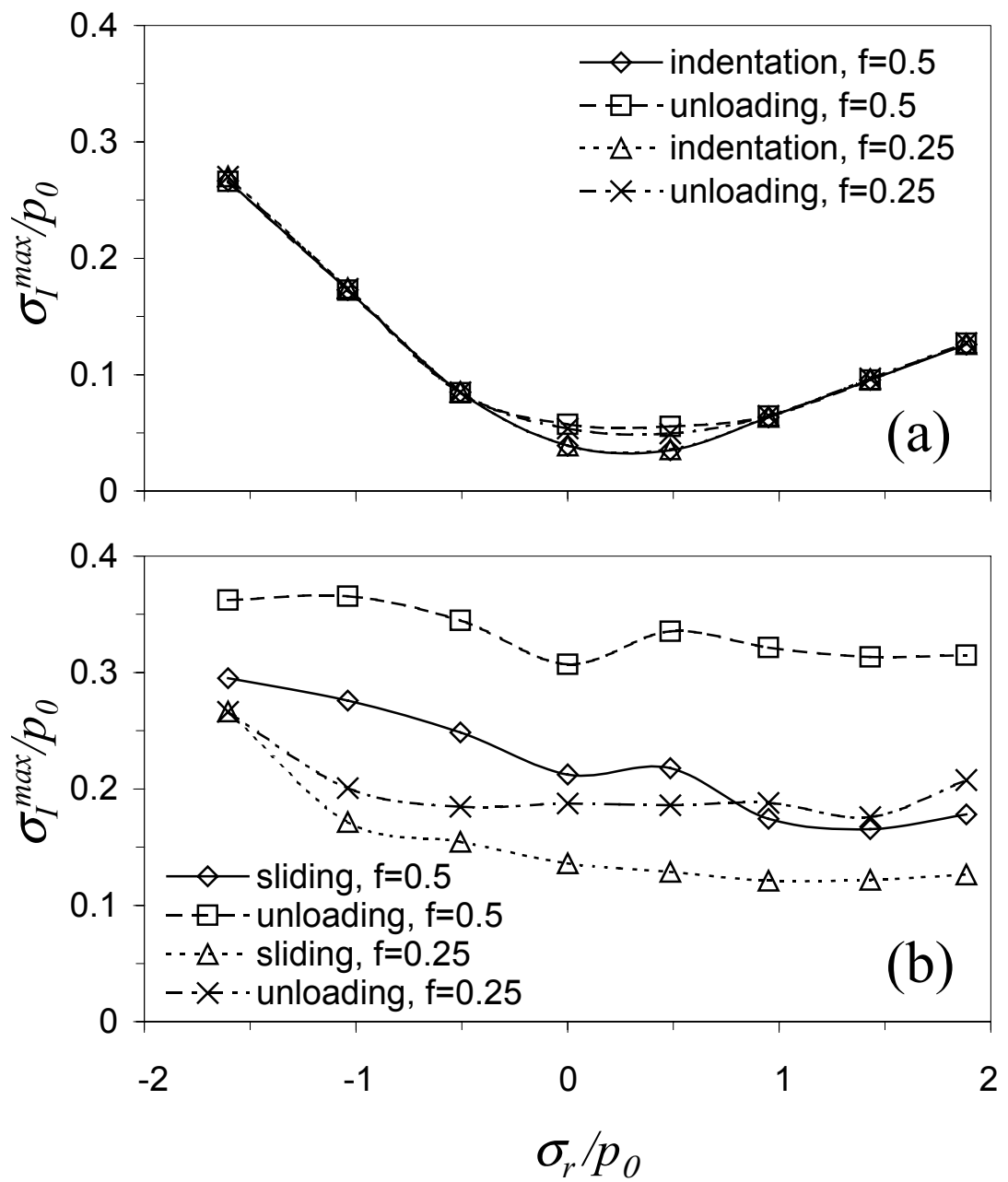
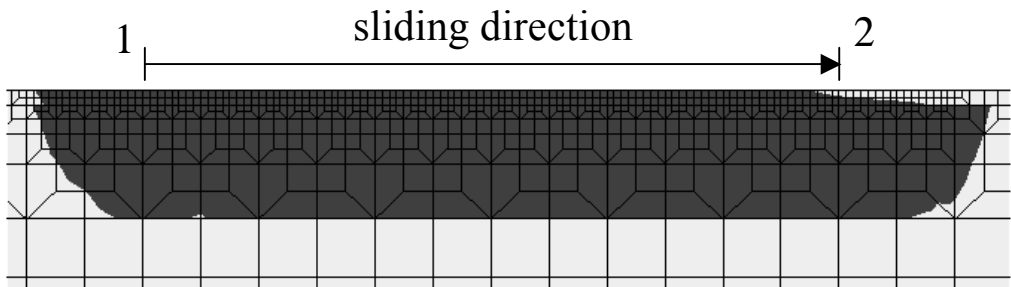
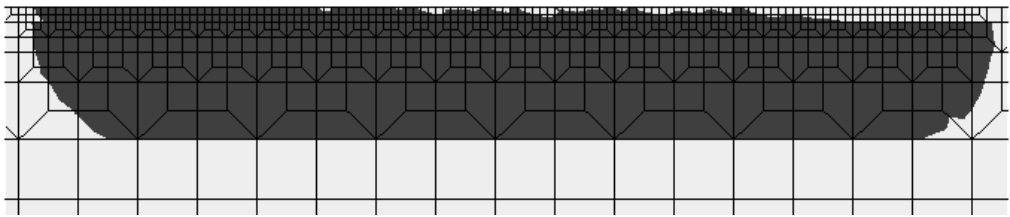


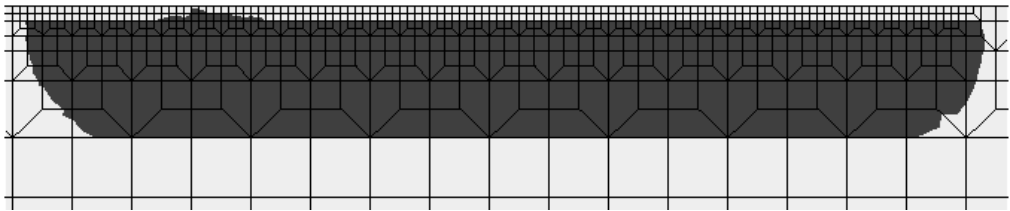
Figure 9



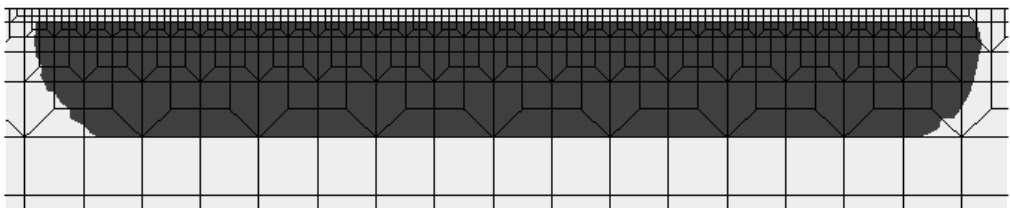
(a) $f = 0.25$, $\sigma_r / \sigma_Y = 0.95$



(b) $f = 0.25$, $\sigma_r / \sigma_Y = 0.75$

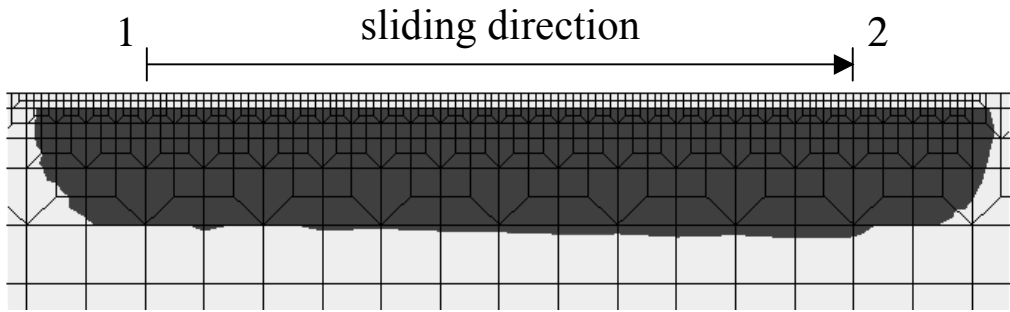


(c) $f = 0.25$, $\sigma_r / \sigma_Y = 0.5$

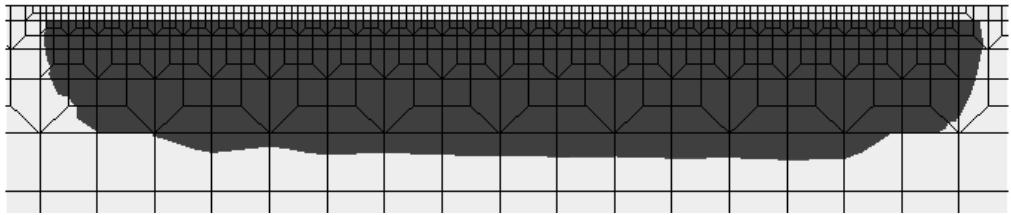


(d) $f = 0.25$, $\sigma_r / \sigma_Y = 0.25$

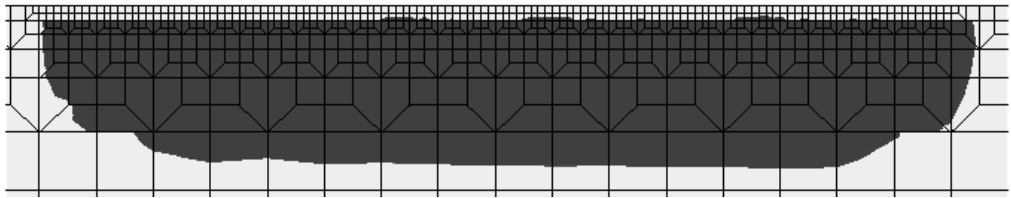
Figure 10



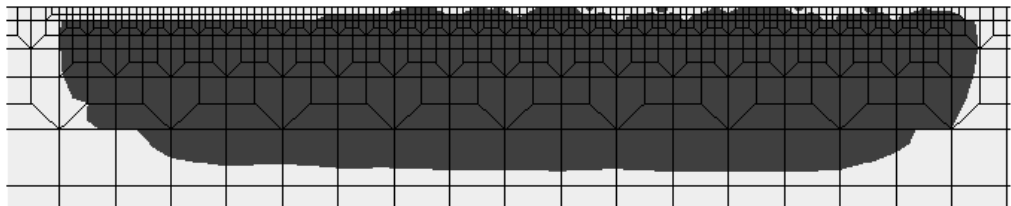
(a) $f = 0.25, \sigma_r / \sigma_Y = 0$



(b) $f = 0.25, \sigma_r / \sigma_Y = -0.25$

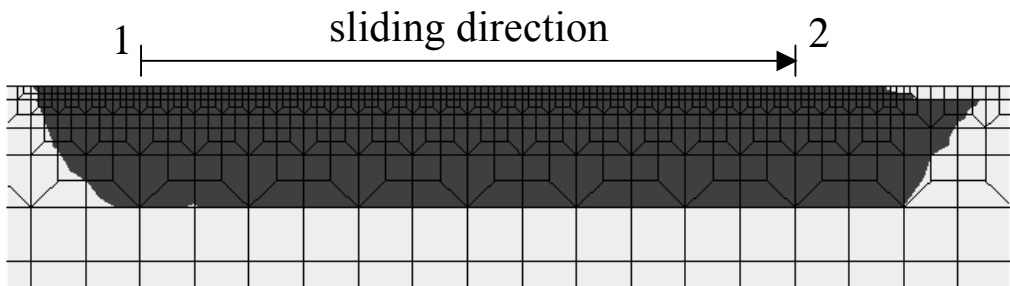


(c) $f = 0.25, \sigma_r / \sigma_Y = -0.5$

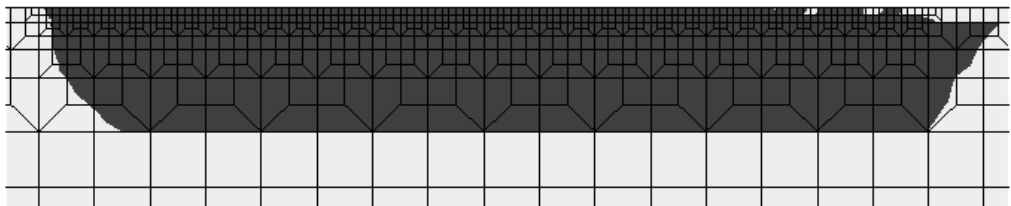


(d) $f = 0.25, \sigma_r / \sigma_Y = -0.75$

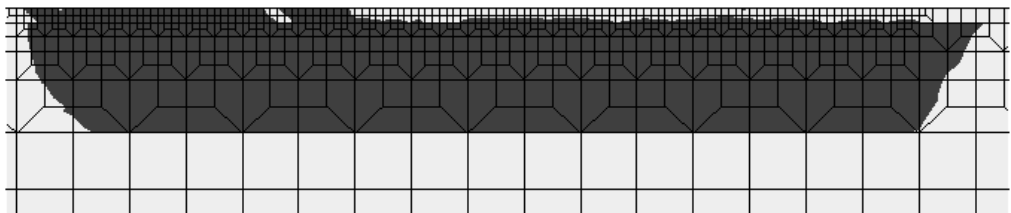
Figure 11



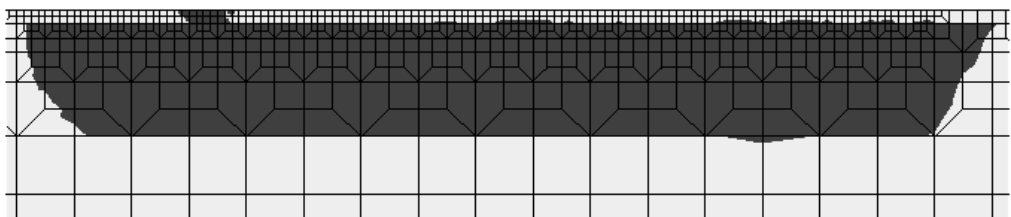
(a) $f = 0.5$, $\sigma_r / \sigma_Y = 0.95$



(b) $f = 0.5$, $\sigma_r / \sigma_Y = 0.75$

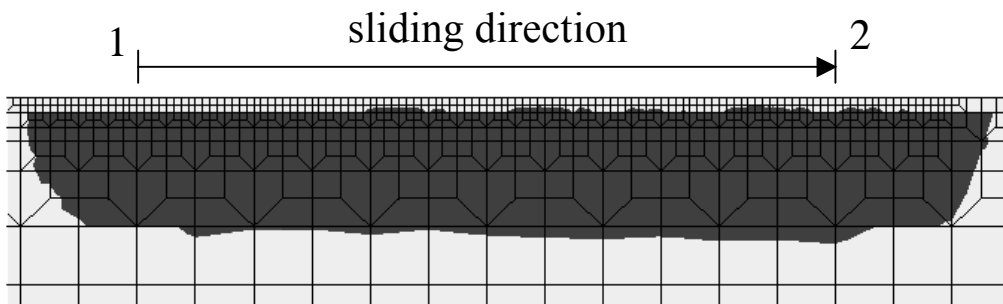


(c) $f = 0.5$, $\sigma_r / \sigma_Y = 0.5$

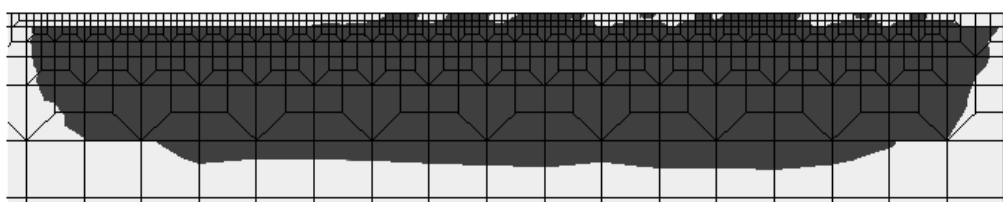


(d) $f = 0.5$, $\sigma_r / \sigma_Y = 0.25$

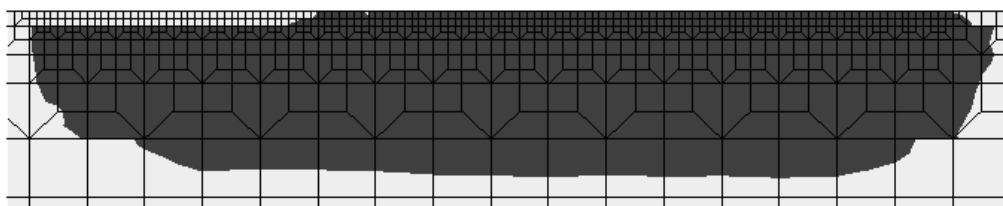
Figure 12



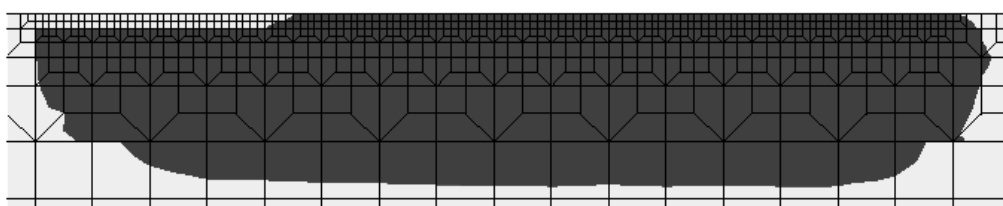
(a) $f = 0.5, \sigma_r / \sigma_Y = 0$



(b) $f = 0.5, \sigma_r / \sigma_Y = -0.25$



(c) $f = 0.5, \sigma_r / \sigma_Y = -0.5$



(d) $f = 0.5, \sigma_r / \sigma_Y = -0.75$

Figure 13